Experimental and numerical analysis of 3D printed open-hole plates reinforced with carbon fibers

Composites Part C: Open Access 2 (2020) 100007

Contents lists available at ScienceDirect

Composites Part C: Open Access

journal homepage: www.elsevier.com/locate/jcomc

Experimental and numerical analysis of 3D printed open-hole plates reinforced with carbon fibers

E. Zappino*, M. Filippi, A. Pagani, M. Petiti, E. Carrera

MUL² Group, Department of Mechanical and Aerospace Engineering, Politecnico di Torino Corso Duca degli Abruzzi 24, Torino 10129, Italy

ARTICLE INFO

Keywords:
Additive manufacturing
Composite
Digital image correlation
Stress mitigation
Open-hole plate,

ABSTRACT

The present work investigates the possibility of reducing the strain/stress concentrations in a open-hole plate using localized 3D printed carbon fiber reinforcements. Several reinforcement strategies have been investigated exploiting the capabilities of a recent additive manufacturing process, the carbon filament fabrication, that allows continuous carbon fibers to be arbitrarily oriented on a plate. Both experimental and numerical investigations have been performed to evaluate the effectiveness of the reinforcements in the mitigation of the strain/stress concentration. The strain fields evaluated during the experimental test, acquired using a digital image correlation technique, have been compared with the results coming from a finite element model. The reliability of the finite element model has been evaluated and its capability to predict the behavior of such complex structures has been checked. The results have shown that the use of an appropriate reinforcement strategy can lead to a considerable reduction in the strain/stress concentration and that an appropriate finite element model can be used to investigate such structures.

Thin-walled structures are used in many engineering fields such as aerospace, automotive or railway. The maintenance requirements, as well as the need to integrate these structures with the other systems, require the presence of cut-outs and holes that may reduce the structural strength as demonstrated by the aircraft Comet I. This aircraft, the first pressurized, experienced many fatigue failures in the fifties due to the stress concentrations around the window cut-outs, see [1]. Since the presence of stress concentrations has a strong impact on the structural design, during the second half of the twentieth century, a large number of theoretical and experimental studies were presented on this topic. The books by Savin [2], Roark [3] and Peterson [4] deserve to be mentioned for their comprehensive analysis of the problem from the phenomenological and numerical points of view. Most of the research activities in this field have been devoted to the analysis of open-hole plates under axial and shear loads. Since the beginning of the last century, see [5], many analytic solutions have been proposed, in many cases using a two-dimensional approximation under the assumption of a plane stress field. The development of advanced structural models, such as the finite element models, has been recently used in many works to obtain a completely three-dimensional solution and to investigate more complex configurations. Mekalke et al. [6] compared the analytic results for stress and displacements around a circular hole with those obtained via FEM for different mesh configurations. Masrol and Siswanto [7] compared the numerical results obtained using elements with four and eight nodes. The effects of many geometrical parameters were also investigated as the width of the plate, the hole diameter and the impact of the plate thickness, see [8] and [9]. The introduction of composite materials has made the evaluation of the stress concentrations more challenging since the orthotropic properties and the multilayered configuration produce complex stress fields. The report by Ko [10] and the work by Toubal et. al. [11] studied the stress distribution in a open-hole composite plate. Khechai et al. [12] studied the effects of the fiber orientation angle on the stress concentration factor and the failure loads for different composite materials. Whitney and Nuismer[13] presented a stress fracture criteria to predict the failure of composite plates with stress concentrations. Many affords have been done in the development of approaches able to mitigate the stress concentration factor in open-hole plates. Meguid [14] proposed the use of additional holes to redistribute the stress field, the use of auxiliary holes have also been proposed by Erickson and Riley [15]. Jindal [16] proposed to modify the hole shape to reduce the stress concentrations. The use of advanced materials has led to new mitigation techniques, the work by Yang and Gao [17] and by Sburlati et. al. [18] propose the use of functionally graded material to minimize the stress concentrations. The use of composite materials with curvilinear fibers, see [19], has allowed optimized reinforcements to be used to reduce local stress peaks. The use of the polar method has led to a convenient description of the stiffness of a general laminate, as shown in the review by Vannucci [20]. This approach has been used for the analysis of laminate structures using a fist order shear deformation

* Corresponding author.
E-mail address: enrico.zappino@polito.it (E. Zappino).

https://doi.org/10.1016/j.jcomc.2020.100007
Received 11 May 2020; Received in revised form 23 July 2020; Accepted 24 July 2020

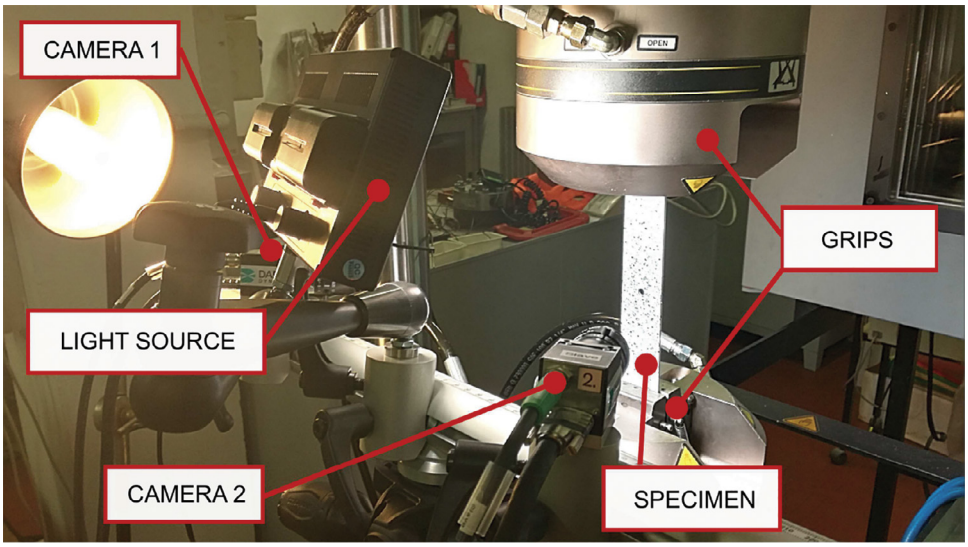

Fig. 1. Digital image correlation.

theory by Montemurro [21]. Montemurro and Catapano [22] exploited the polar formalism to develop a two-level optimization approach for variable angle tow laminates.

The works by Crothers et. al. [23] and Gliesche et. al. [24] presented the use of the automatic fiber placement techniques to reinforce the open-hole plates with a consequent reduction of the stress singularities. Additive manufacturing techniques, such as the fused filament fabrication (FFF) and the carbon filament fabrication (CFF), allow continuous carbon fibers to be included in polymeric component as shown in [25,26]. The improvement of the mechanical response of simple coupons due to the introduction of the reinforcements has been demonstrated in [27,28].

The present work investigates the use of carbon fiber reinforcements to mitigate the stress concentration. The use of a recent manufacturing process, based on the additive manufacturing technique, has allowed arbitrary reinforcements to be created in the open-hole plate. Experimental tests, analytic and numerical analyses have been performed. The specimens have been produced by means of the 3D printer *MarkTwo*® provided by *Markforged*® and they have been tested under a uni-axial load. The digital image correlation technique, DIC, has been used to evaluate the strain field during the test, see [29,30]. The results have been used to validate a classical finite element model.

The paper is organized as follow. At first the experimental setup and the numerical approach have been presented. Then, the numerical model and the experimental setup have been validated through an assessment with close form solutions available in the literature. Both isotropic and orthotropic plates have been considered. In the second part, different reinforcing approaches have been investigated both numerically and experimentally.

1. Experimental setup

Fig. 1 shows the test facilities used to perform the traction test. The specimens have been tested using an Instron 8516 testing system that provides a traction/compression maximum force equal to 100 kN. The results have been acquired by means of a Q-400 Digital Image Correlation, DIC, system by Dantec Dynamics whose optical features allow to measure true full-field, non-contact and three-dimensional shape, displacements and strains on components and structures made from almost any material. This apparatus, as shown in Fig. 1, is made of two 2-megapixel cameras for high-frequency image tracking, one light source, the supporting structure, the data acquisition unit, and the calibration tool. Image processing, on the other hand, is performed with the licensed Instra4D V2.1 software tool.

The specimens have been manufactured by means of the 3D printer Mark Two produced by Markforged. The printer is shown in Fig. 2a, while Fig. 2b shows the apparatus during the printing procedure.

1.1. 3D printing manufacturing process

The specimens object of the present work have been produced by means of a fused deposition modeling (FDM) approach. The used 3D printer has the capability to deposit continuous carbon fibers that can be used to reinforce the component made of a polymeric material, in this case, nylon. This technique allows the fibers to be oriented with a different strategy in each layer of the component. Different reinforcement strategies can be adopted. The fibers can be placed unidirectionally, see Fig. 3a, or along the inner/outer border of the layer, see Fig. 3b. The two strategies can be mixed together, as shown in Fig. 3c. Fig. 4 shows a schematic view of a 3D printed structure. The printing approach requires to place at the least two lateral polymeric walls around the border of each layer. At least four layers of polymeric material should be placed at the bottom, floor, and at the top, roof, of the component. The filling can be arbitrarily defined using different fiber reinforcement strategies, solid fill or honeycomb. Each layer can have a thickness of 0.1, 0.125 or 0.2 mm. When the carbon fiber reinforcements are used, the thickness of the layer is driven by the fiber, that is, a value of 0.125 mm must be used. Fig. 5 shows the details of the printed fiber. Each tow has an average width of 1 mm, a thickness of 0.125 mm and is composed of thousands of fibers with a diameter of 8 μm.

2. Numerical modeling

Closed-form solutions and numerical models have been used to reproduce the experimental results. Analytic solutions have been exploited to assess the numerical models for both pure nylon and carbon-reinforced nylon specimens. The analysis of unconventional reinforced specimens has been carried out by using the numerical approach only since the complexity of the fiber setup does not allow analytic formulations to be used.

2.1. Closed-form solution

The analysis of the stress concentration factors in a open-hole plate has been investigated exhaustively in the sixties. The theoretical derivation of the stress intensity factor for an arbitrary hole can be found in many books, e.g. see [3,4]. It is well known that, when an isotropic open-hole specimen undergoes to a traction load, a stress concentration

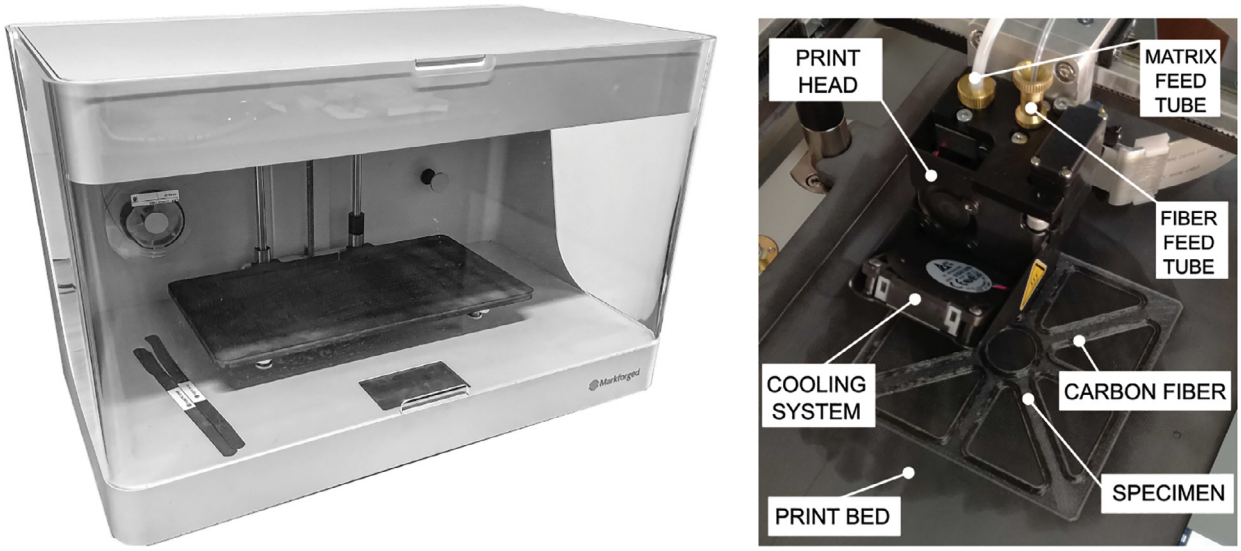

(a) 3D printer. (b) Printing procedure

Fig. 2. 3D Printer apparatus.

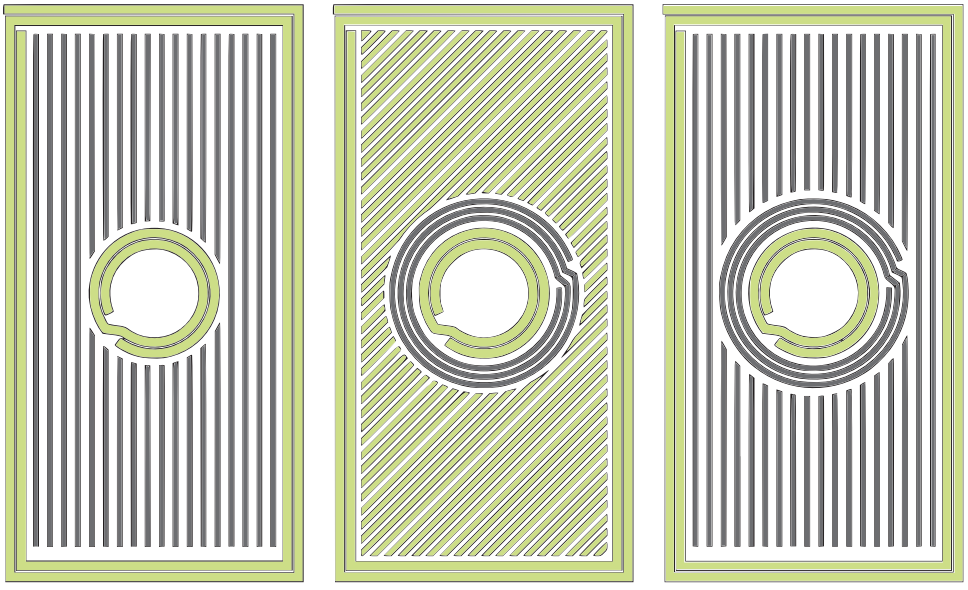

(a) Unidirectional (b) Concentric (c) Mixed

Fig. 3. Schematic representation of the fiber reinforcement strategies. The green zones represent the polymer, while the gray regions represent the fibers.

appears. Fig. 6 shows that, if σ_{xx} is the axial sigma applied, the stress at point A increases of an intensity factor named K_σ while the axial stress at point B becomes zero to respect the boundary conditions.

The stress intensity factor,K_σ, depends on many geometrical and physical parameters, for an exhaustive review see [31]. The formulations reported in [4], for the isotropic material, and in [10], for the composite, have been used in this work. The comparisons between the experimental data and the numerical results have been performed through the strain intensity factor, which is defined as:

$$K_\varepsilon = \frac{\varepsilon}{\varepsilon_0} \tag{1}$$

where ε_0 is the unperturbed axial strain. As far as the experiments are concerned, the strain intensity factor has been computed with ease, since the strain fields of specimens were directly provided by the adopted acquisition system.

2.2. Finite element modeling

The commercial code Nastran has been used to develop the Finite Element models of the specimens considered in the present work. The models have been created using 4-node plate elements. Different mesh refinement strategies have been considered in order to capture the local effects properly at the hole edge.

Fig. 7 shows the meshing strategies considered in the present work. Since the stress concentration appears close to the hole edge, the use of a uniform mesh, see Fig. 7a, requires a huge computational cost. A refinement of the area around the opening can be obtained using a washer, see Fig. 7b, that creates a refined and regular mesh around the hole. Finally, a box has been included around the washer, see Fig. 7c, in order to obtain a regular mesh everywhere and to increase the quality of the mesh in the transition from the washer to the outer zone of the specimen.

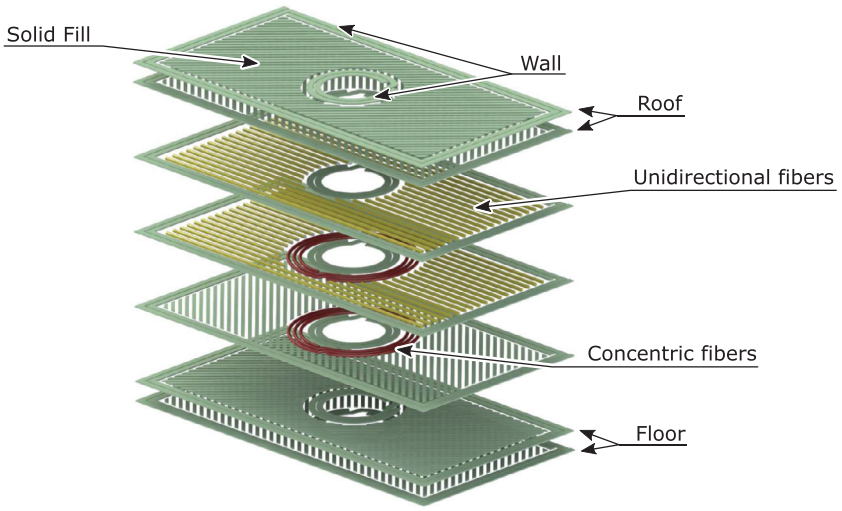

Fig. 4. Exploded view of a 3D printed structure.

(a) View of printed fiber tow. (b) Details of the fiber tow

Fig. 5. Microscope images of the printed fibers.

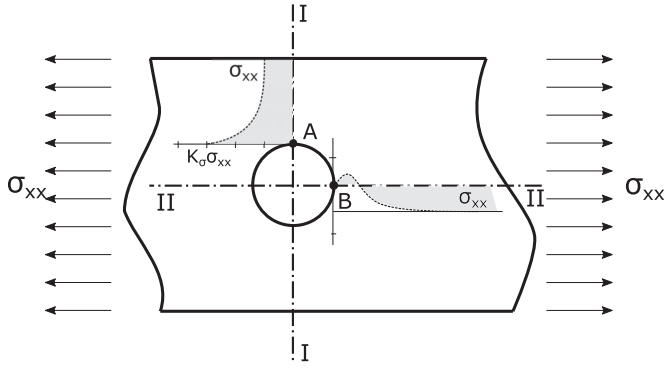

Fig. 6. Axial stress distribution in a open-hole plate.

When the circular reinforcements have to be included in the model, as shown in Fig. 3b, the proper choice of the washer geometry allows the right lamination angle to be assigned in the area around the hole, as shown in Fig. 7d, where the red elements have a lamination that includes the fibers.

The performances of the three meshes approaches have been compared. The value of the stress concentration factor in an isotropic open-hole plate has been evaluated using the three different approaches and compared with the analytic solution. The results reported in Table 1 show that all three the approaches ensure an accurate solution but, the local refinement obtained using the washer and the controlled transition obtained using the washer & box, reduces the computational costs if compared with the uniform mesh. Considering these findings, the mesh with washer & box has been used in the following analysis. The materials have been considered to have a linear elastic behavior. This assumption is generally not verified for plastic materials. The use of a low external load, an pause between the load steps and before the data acquisition (to avoid viscoelastic effects) and a low strain rate make the use of a linear model acceptable for the scope of the present paper.

3. Results

In this section, the experimental results are compared with the results obtained using the numerical approaches introduced. Specimens with different reinforcement strategies are compared, the following models have been considered:

- Isotropic open-hole plate (ISO)
- Isotropic open-hole plate with concentric reinforcements (ISO-R)
- Composite open-hole Plate (COMP)
- Composite open-hole plate with concentric reinforcements (COMP-R)

For each configuration two specimens have been tested. All the specimens have been printed with a layer thickness of 0.125 mm. The models have been created considering a one-layer wall. The details of the stacking sequences have been reported in Table 2. The material deposition strategies are reported in Fig. 8.

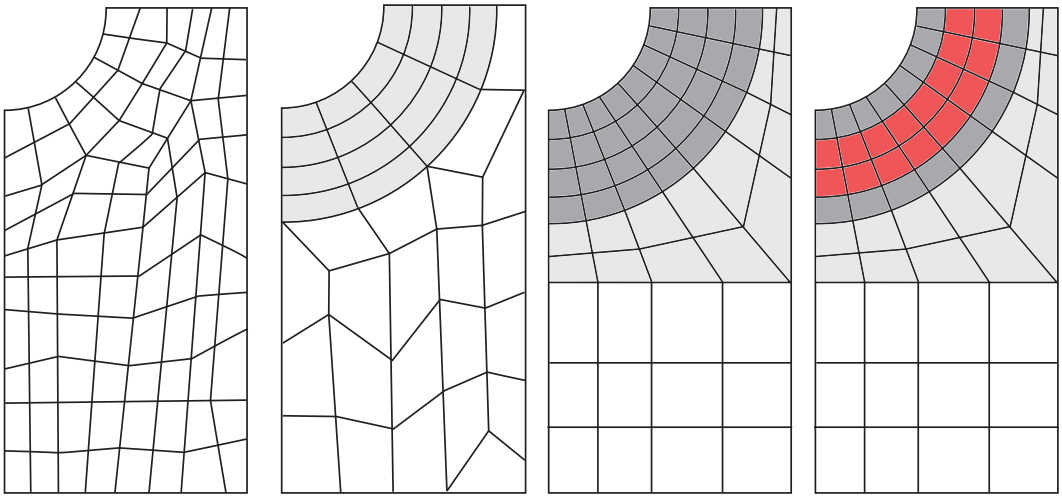

(a) Uniform Mesh. (b) Washer. (c) Washer and box. (d) Circular reinforcements.

Fig. 7. Meshing strategies used in the assessment of the numerical approach.

Table 1
K_σ evaluated using different mesh strategies.

	Closed Form Solution	Uniform Mesh	Washer	Washer & Box
K_σ	3.0944	3.0930	3.0910	3.0910
Error %	-	0.05%	0.11%	0.11%
Solution time [s]	-	40	12	8

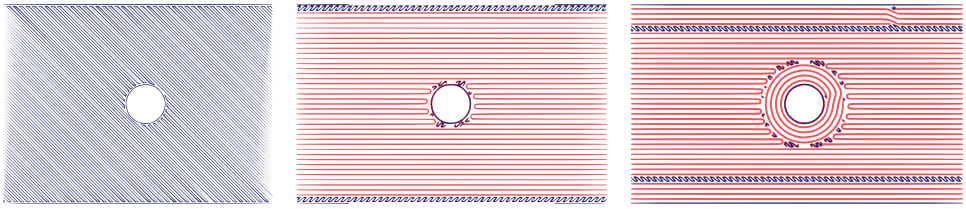

Fig. 8. Material deposition strategies: isotropic, unidirectional carbon fiber and reinforced unidirectional carbon fiber. Nylon in blue and fibers in red.

Table 2
Stacking sequence details: ISO - Isotropic; CR - Concentric Reinforcements; UCF - Unidirectional carbon fiber.

	Specimens			
Layers	ISO	ISO-R	COMP	COMP-R
1-8	ISO	ISO	ISO	ISO
9-12	ISO	ISO + CR	UCF	UCF + CR
13-20	ISO	ISO	ISO	ISO

The geometry of the specimens follows the recommendation proposed in [32]. Table 3 shows the nominal and real values of the geometry of the specimen.

The tests have been carried out increasing the axial load step-by-step. The data have been acquired using the DIC system, presented in Section 1, at each step. A load step of 500 N has been used for the isotropic coupons while a step of 1000 N has been used for the composite plates. A strain ratio of 0.001 1/s has been used for models ISO and ISO-R while a strain ratio equal to 0.00025 1/s has been used for the composite specimens. Fig. 9 shows the specimens before the testing, white background with a black pattern has been used for the DIC acquisition.

3.1. Isotropic plate

The first analysis concerns the isotropic coupons. Closed-form solution, numerical and experimental results have been compared in order to assess the experimental setup and the numerical model. Fig. 10 reports the axial strain field for a load of 1500N. The numerical and experimental results agree, and the FEM model can capture all the strain concentrations, as depicted in the contour maps. The maximum axial strain, as expected, appears close to the hole. The quantitative evaluation of the results along the transverse and longitudinal sections, as shown in Fig. 6, is reported in Fig. 11. The results show a good agreement between the closed-form solution, the FEM model and the experimental results. The maximum stress/strain intensity factor is close to 3, in accord with the results presented in the literature, see [31]. The closed-form solution has been used as a reference, and the results confirm the accuracy of the FEM model adopted and the reliability of the experimental setup.

3.2. Reinforced isotropic plate

This section investigates the use of circular carbon fiber reinforcements to reduce the strain concentrations around the open hole. Fig. 12 shows the specimen ISO-R 2 before to be treated for the DIC acquisition. Models ISO-R 1 and 2 have been reinforced with four loop of carbon fiber around the hole and 4 layers of reinforcements through the

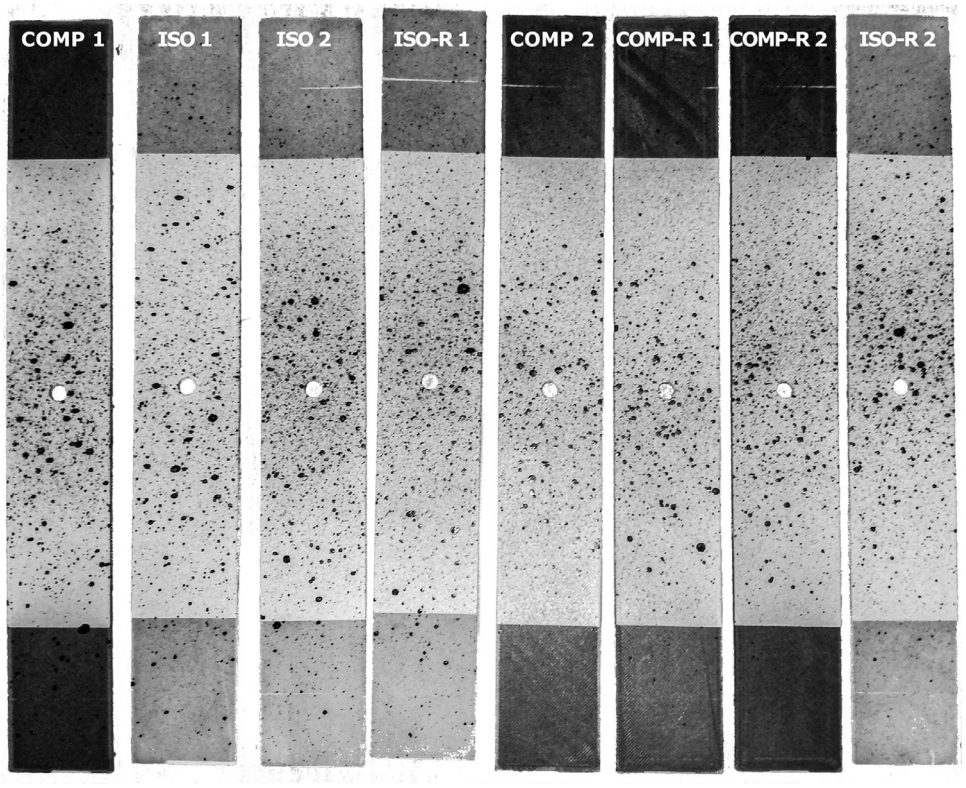

Fig. 9. Specimens before the testing.

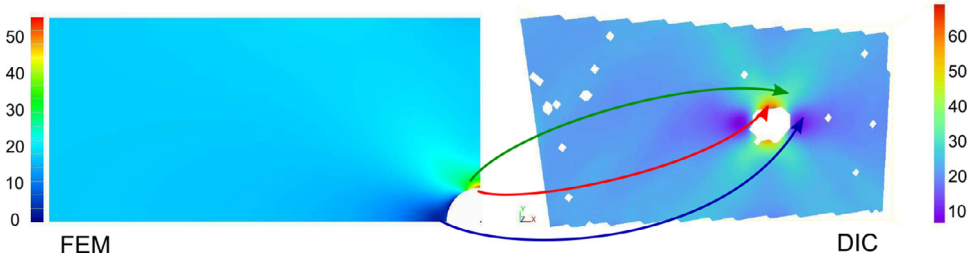

Fig. 10. Unreinforced isotropic plate. Axial strain field, $[m\varepsilon]$, at 1500$[N]$. Comparison between numerical and experimental results (specimen ISO 1).

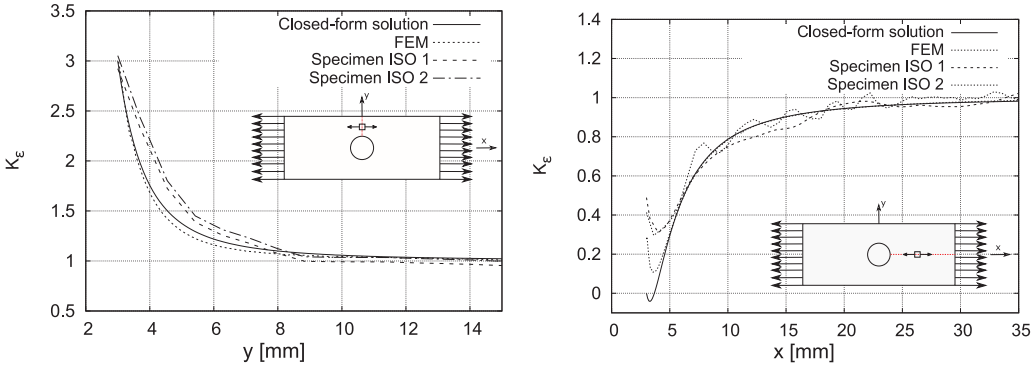

(a) Transverse section (b) Longitudinal section

Fig. 11. Strain intensity factor for the isotropic plates. Comparison between closed-form solution, FEM model and experimental results.

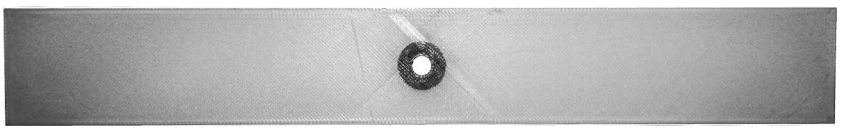

Fig. 12. Isotropic plate with carbon fiber reinforcements, specimen ISO-R 2 before to be treated for the DIC acquisition.

Table 3
Specimens nominal and real geometry.

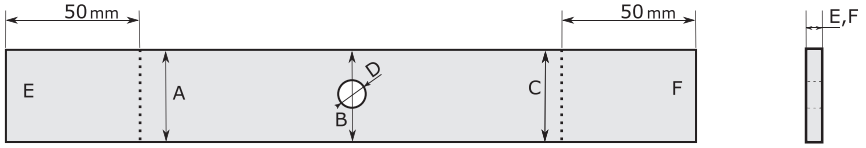

Specimen	A [mm]	B [mm]	C [mm]	D [mm]	E [mm]	F [mm]
Design	36.00	36.00	36.00	6.00	2.50	2.50
ISO 1	35.85	35.73	35.70	6.10	2.35	2.53
ISO 2	35.83	35.63	35.70	6.11	2.57	2.48
ISO-R 1	35.68	35.67	35.78	6.11	2.62	2.62
ISO-R 2	35.80	35.90	35.86	6.10	2.64	2.59
COMP 1	35.82	35.82	35.81	5.75	2.32	2.53
COMP 2	35.74	35.81	35.83	5.94	2.53	2.44
COMP-R 1	35.73	35.78	35.74	6.10	2.35	2.47
COMP-R 2	35.77	35.84	35.84	6.07	2.44	2.58

Specimen	A [mm]	B [mm]	C [mm]	D [mm]	E [mm]	F [mm]
Design	36.00	36.00	36.00	6.00	2.50	2.50
ISO 1	35.85	35.73	35.70	6.10	2.35	2.53
ISO 2	35.83	35.63	35.70	6.11	2.57	2.48
ISO-R 1	35.68	35.67	35.78	6.11	2.62	2.62
ISO-R 2	35.80	35.90	35.86	6.10	2.64	2.59
COMP 1	35.82	35.82	35.81	5.75	2.32	2.53
COMP 2	35.74	35.81	35.83	5.94	2.53	2.44
COMP-R 1	35.73	35.78	35.74	6.10	2.35	2.47
COMP-R 2	35.77	35.84	35.84	6.07	2.44	2.58

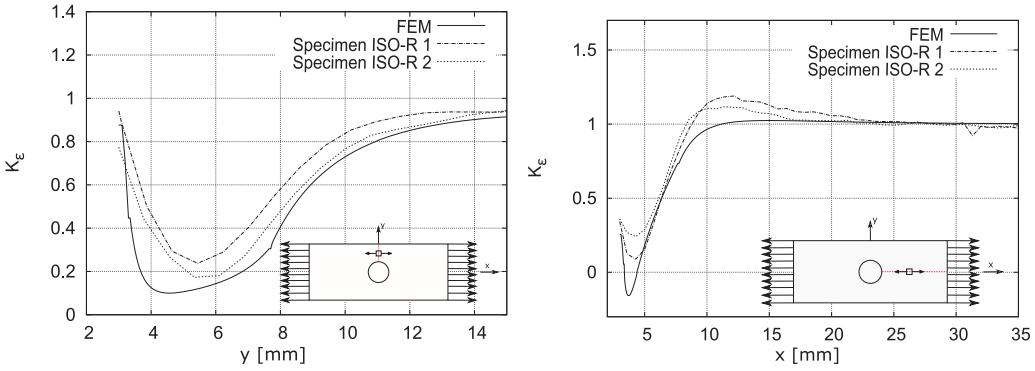

(a) Transverse section (b) Longitudinal section

Fig. 13. Strain intensity factor for the reinforced isotropic plates. Comparison between FE model and experimental results.

thickness. The results coming from the experimental test, with a load of 1500 N, have been compared with those from the numerical FE model.

Fig. 12 shows the intensity factor evaluated in the transverse and longitudinal sections. The strain intensity factor along the transverse section, Fig. 13(a), shows a significant reduction in its value, with respect to the isotropic panel. The value of K_ε is always lower than one. The results obtained with the DIC confirm those from the FEM Model and demonstrate the effectiveness of the concentric carbon fiber reinforcements in the reduction of the strain concentration. The longitudinal distribution of K_ε, see Fig. 13(b), shows a distribution comparable with the unenforced model. The value is equal to one up to the reinforcement area where it drops to a value close to zero.

The axial strain distributions evaluated using the numerical model and the DIC have been compared in Fig. 14. The numerical solution is able to reproduce with accuracy the experimental result. The strain field is strongly afflicted by the presence of the carbon fiber reinforcements and the differences between this model and the isotropic model are significant, see Fig. 10. A strong reduction of the axial deformation

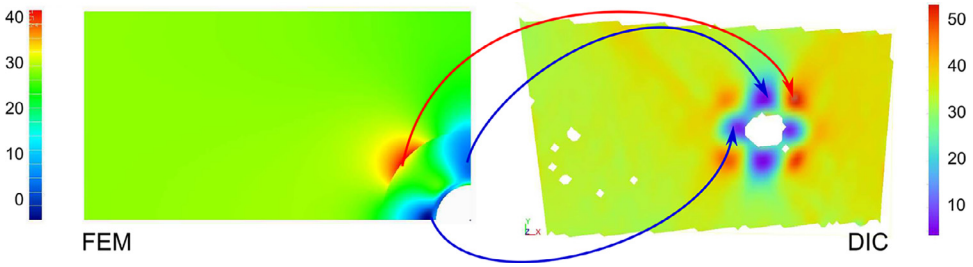

Fig. 14. Reinforced isotropic plate. Axial strain field, [$m\varepsilon$], at 1500[N]. Comparison between numerical and experimental results (specimen ISO-R 2).

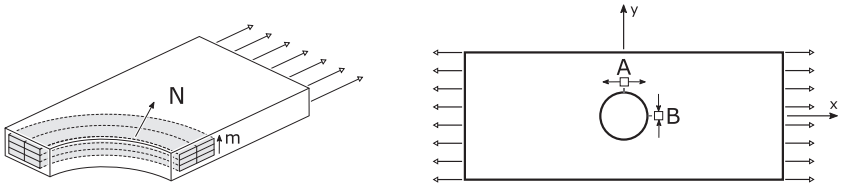

(a) Trasversal section (b) Longitudinal section

Fig. 15. Characteristic points in plates

appears all around the hole, but a new strain concentration appears at the boundary between the fibers and the isotropic panel, denoted in the picture by the red areas.

The results prove the reliability of the numerical approach in the prediction of the effects of the carbon fiber reinforcements. The same modeling technique has been used in the following sections to investigate the effect of the circumferential and through-the-thickness number of reinforcements.

3.2.1. Effect of the number of concentric reinforcements

This section investigates the effect of the number of concentric carbon fiber reinforcements of the stress/strain concentrations. Fig. 15a shows the two parameters, N and m, that have been considered to define the reinforcement strategy. N is the number of concentric carbon fiber reinforcements while m is the number of layers in which the reinforcements have been placed. According to this notation, when a model whit $N = 2$ and $m = 4$ is considered, the spacemen is reinforced with 4 layers of 2 concentric loop of carbon fiber. The numeric results have been evaluated at points A and B, as shown in Fig. 15b.

At first, m has been considered fixed and equal to 4 and the number of concentric reinforcements, N, has been varied between 2 and 7. Fig. 16 reports the map of the axial strain concentration factor for the un-reinforced model, and the models reinforced with 2, 4 and 7 concentric lops of carbon fiber. The results show a significant reduction in the concentration factor when the reinforced models are considered. The maximum value, equal to 3.11 for the reinforced models, becomes 1.59 when $m = 2$ and it becomes smaller when m increases.

Fig. 17 shows the axial stress field for the model $m = N = 4$. As expected, the carbon fiber reinforcements undergo larger axial stress since they are much stiffer than the polymeric material. Considering the axial load applied equal to 1 [MPa], the polymeric matrix has shown maximum axial stress equal to 1.34 [MPa]. Table 4 shows the hoop stress value at points A and B for the models considered. When the number of concentric reinforcements is increased, the stress at point A decreases while the hoop stress at B slightly increases.

The same analysis has been conducted with a fixed number of concentric reinforcements, $N = 4$, and considering a variable number of reinforced layers, m, from 4 to 12 (Table 5). The results show that the number of reinforced layers has a significant effect on the stress reduction both at points A and B. When 12 reinforced layers are used instead 4, the stress value is reduced of about 50% in both points.

In order to clarify which parameter, N or m, has the most significant effect of the stress concentration mitigation, the results have been compared in terms of the reinforcements section. Each carbon fiber has a section of about 0.137 mm^2, the total reinforcements section has been evaluated as $A_r = N \times m \times 0.137$.

Table 4
Hoop stress at points A and B for different reinforcement configurations. The stress is evaluated at the mid plane in the inner carbon fiber reinforcement. $m = 4$.

N (m=4)	σ_θ at A [MPa]	σ_θ at B [MPa]
2	29.12	-17.68
3	26.64	-19.33
4	25.22	-20.19
5	24.30	-20.66
6	23.67	-20.95
7	23.23	-21.13

Table 5
Hoop stress at points A and B for different reinforcement configurations. The stress is evaluated at the mid plane in the inner carbon fiber reinforcement. $N = 4$.

m (N=4)	σ_θ at A [MPa]	σ_θ at B [MPa]
4	25.22	-20.19
6	19.57	-17.23
8	16.32	-15.09
10	14.15	-13.46
12	12.57	-12.16

Table 6 shows the hoop stress at points A and B considering models with a different number of reinforcements. The third column reports the total area of the reinforcements. The same results have been graphically reported in Fig. 18, the models have been denoted using the code (N,m). The results clearly show that for a given reinforcements section, the solution with a lower number of circumferential reinforcements and with more reinforced layers gives a lower stress concentration. As an example, it can be observed that 2 models have a section of 5.5 mm^2, the first is the model (4,10) and the second is model (5,8). The comparisons reveals that model (4,10) provided lower hoop stresses at points A and B than the model (5,8). From the present results, it can be concluded that it is more convenient to introduce the reinforcements close to the hole increasing the number of reinforced layers, m, instead of introducing more concentric reinforcements, N.

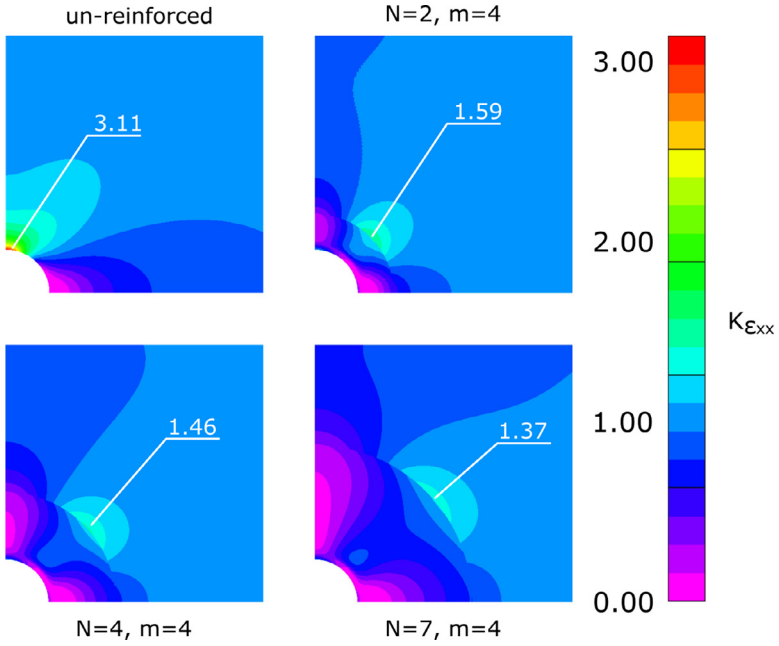

Fig. 16. Axial strain concentration factor, $K_{\varepsilon_{xx}}$, for different models. Results evaluated at the top surface.

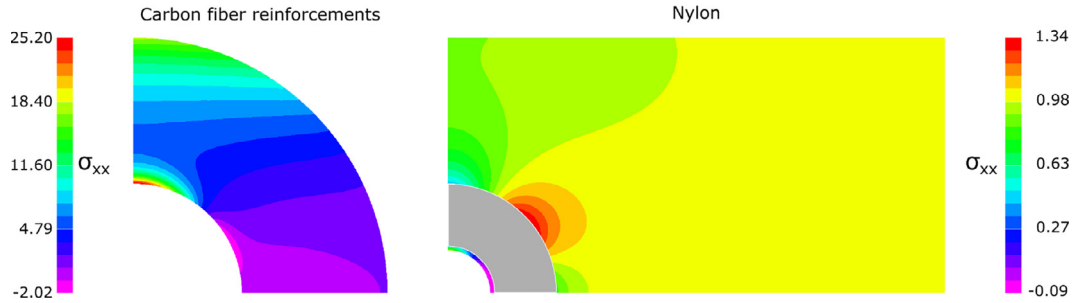

Fig. 17. Axial stress field, [MPa], for the model $m = N = 4$. Results evaluated at the mid-plane of the specimen.

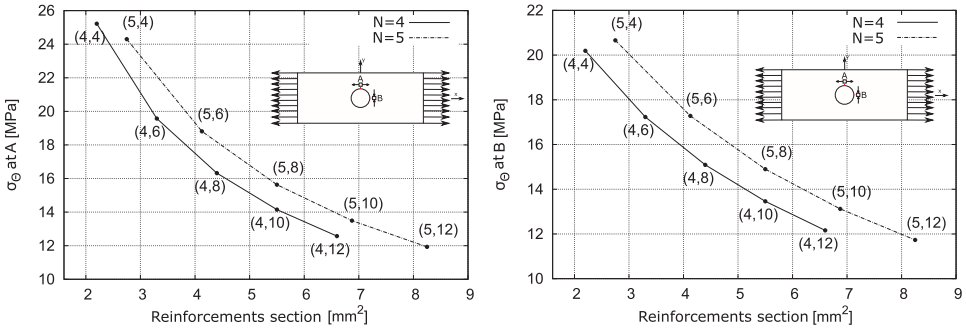

(a) σ_θ at A (b) σ_θ at B

Fig. 18. Hoop stress VS reinforcement section. Each models is denoted using the notation (N,m).

3.3. Composite plate

The stress and strain distributions for a unidirectional composite plate have been investigated, and the results have been reported in this section. The experimental results obtained during the test of the specimen COMP 1 and COMP 2 have been compared with a numerical and a closed-form solution. The model has the same geometry of the isotropic plate, and the fibers are placed in the longitudinal direction. According to the 3D printer capabilities, it must be pointed out that the first and the last four layers are made of nylon. Fig. 19(a) and (b) report the longitudinal strain concentration factor for the transverse and longitudinal sections, respectively. The use of the composite material makes the strain concentration much larger in the area nearby the hole when the transverse section is considered. The longitudinal section shows that the effects of the hole are significant even far from the singularity. This is confirmed by the results shown in Fig. 20 where the strain field evaluated by means of the FE model is compared with the experimental results. The contour maps show a very localized peak in the strain value, the numerical results are confirmed by the good correlation with the DIC output. The dark blue area shows the fibers that are interrupted by the presence of the open hole. The longitudinal strain in these fibers is much lower, as shown in Fig. 19(b).

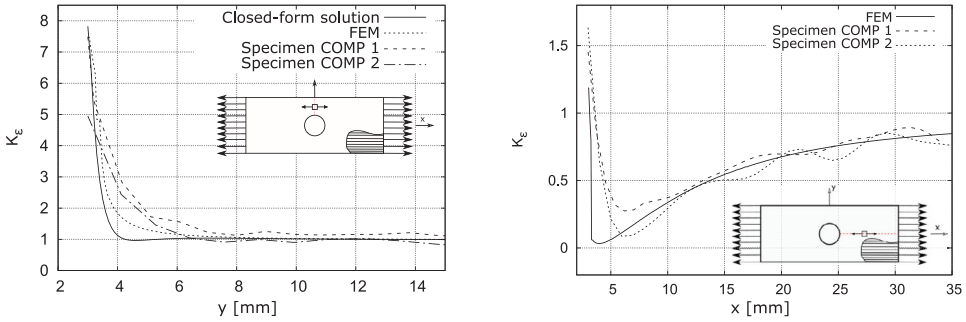

(a) Transverse section (b) Longitudinal section

Fig. 19. Strain intensity factor for the composite plates. Comparison between closed-form solution, FEM model and experimental results.

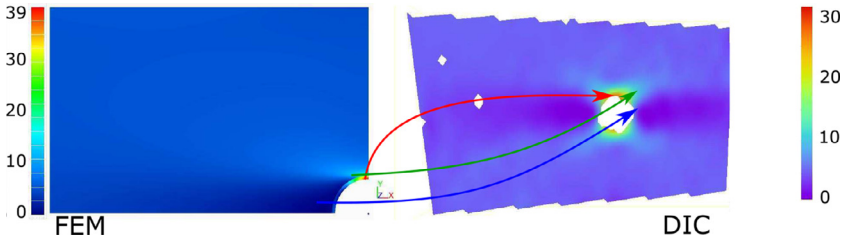

Fig. 20. Composite plate. Axial strain field, $[m\varepsilon]$, at a load of 6000$[N]$. Comparison between numerical and experimental results (specimen COMP-R 1).

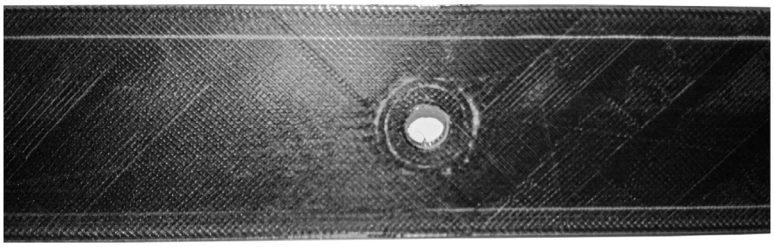

Fig. 21. Reinforced composite plate, COMP-R 1.

Table 6
Hoop stress at points A and B for different reinforcement configurations.

N	m	A_r $[mm^2]$	σ_θ at A [MPa]	σ_θ at B [MPa]
4	4	2.200	25.22	-20.19
5	4	2.750	24.30	-20.66
4	6	3.300	19.57	-17.23
5	6	4.125	18.81	-17.28
4	8	4.400	16.32	-15.09
5	8	5.500	15.63	-14.90
4	10	5.500	14.15	-13.46
5	10	6.875	13.49	-13.12
4	12	6.600	12.57	-12.16
5	12	8.250	11.93	-11.73

3.4. Reinforced composite plate

The high strain concentration found in the composite plate makes the use of circumferential reinforcements of interest since they could mitigate the singularity effects. In this section, the composite plate has been reinforced with four concentric loops of carbon fiber around the hole. The reinforcements have been placed on all the layers except the first and last four, as required by the 3D printer. A view of the reinforced area of the first specimen, COMP-R 1, is reported in Fig. 21. The results in Fig. 22 show that the concentric reinforcements reduce the longitudinal strain peak nearby the hole but determine a new peak at the boundary between the unidirectional carbon fibers and the reinforced area. The present numerical approach is able to predict the strain concentrations even if, the complexity of the specimen, makes the correlation not as good as for the previous cases. The most significant effect can be observed in the longitudinal section, see Fig. 22(b), where at the interface between reinforced area and the unidirectional fibers, the strain concentration seems to be quite severe. The comparison of the contour maps of the axial strain field coming from the numerical analysis and the experimental results is reported in Fig. 23. The two strain fields are in good agreement, the localized strain concentration observed in the composite plate is now replaced by a more distributed strain intensification in the reinforced area. The peak appears at the boundary between the reinforcements and the composite plate, rotated of 45° with respect to the composite plate. Even if the use of the concentric reinforcements has led to a general reduction in the magnitude of the strain concentration, it should be noticed that the new concentrations appear in a weak area, at the boundary between two different lamination strategies. This new phenomenon has a significant impact on the failure mode of the components. Fig. 24 reports the picture of the COMP-1 and COMP-R 2 at the ultimate load. As expected, the failure of the composite plate is due to the strain concentration and takes place in the hole area. Conversely, the reinforced composite panel fails at the interface between the reinforcements and the unidirectional fibers. This difference can also be observed in the value of the failure loads, the specimen COMP 2 failed at 8.8 kN while the plate COMP-R 2 failed at 7.9 kN. A hybrid reinforcements strategy, alternating full composite layers and reinforced composite layers could mitigate this effect and avoid undesired strain concentrations in weak areas.

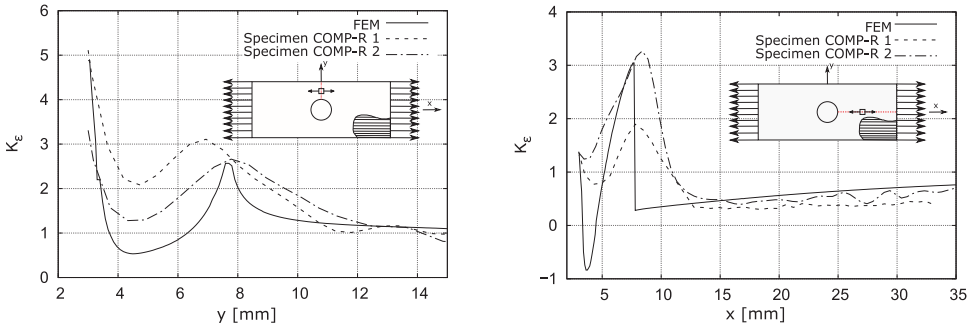

(a) Trasverse section (b) Longitudinal section

Fig. 22. Reinforced composite plate. Axial strain field, $[m\varepsilon]$, at a load of 6000$[N]$. Comparison between numerical and experimental results (specimen COMP-R 2).

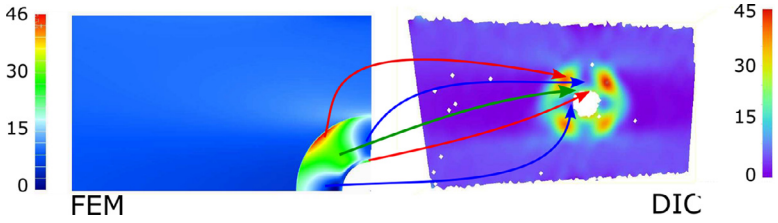

Fig. 23. Strain comparison for reinforced composite plate.

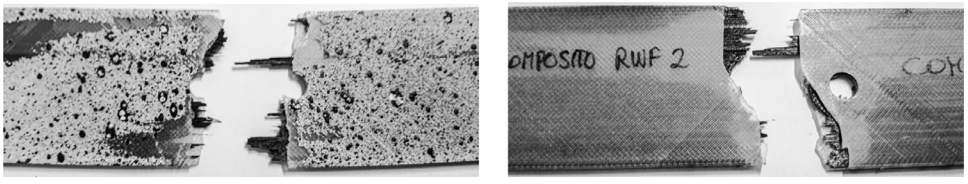

(a) COMP 1 (b) COMP-R 2

Fig. 24. Un-reinforced and reinforced composite plates failure modes.

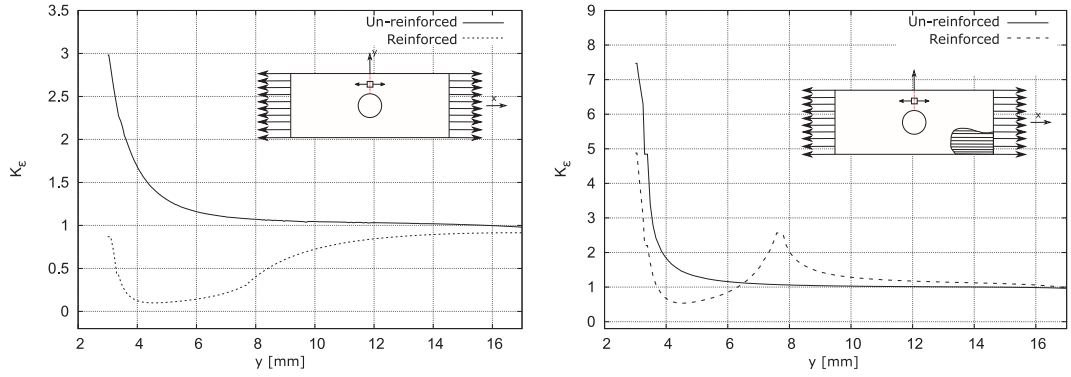

(a) Isotropic plate (b) Composite plate

Fig. 25. Axial strain concentration factor at the strasversal section. Comparison between un-reinforced and reinforced configurations.

4. Conclusions

The aim of this work was to explore the possibility of using the capabilities of the additive manufacturing of composite materials to mitigate the stress and strain concentrations in open-hole plates. The use of the carbon filament fabrication 3D printing technique has allowed standard open-hole plates to be created introducing different reinforcements around the hole. Isotropic and anisotropic plates have been considered. Experimental results, numerical models and, where available, closed-form solutions have been compared to confirm the capabilities of the classical Finite Element Method in predicting the complex strain field due to unconventional reinforcement configurations. The correlation between the FEM models and the experimental data has demonstrated that the present modeling approach is able to predict the strain concentration, even if complex reinforcements configurations have to be considered.

The effect of the introduction of the reinforcement can be observed in Fig. 25. The introduction of concentric reinforcements around the hole has shown a beneficial effect on the strain and stress concentration in the isotropic plate, see Fig. 25a. The use of the same reinforcement strategy in the composite plate, see Fig. 25b has led to a mitigation of the strain peak in the transverse section, where usually the strain concentration

Table A7
Mechanical properties: Nylon.

Tensile Modulus	GPa	0.94
Tensile Stress at Yield	MPa	31
Tensile Strain at Yield	%	27
Tensile Stress at Break	MPa	54
Tensile Strain at Break	%	260
Flexural Strength	MPa	32
Flexural Modulus	GPa	0.84
Density	g/cm^3	1.1

Table A8
Mechanical properties: Carbon Fibers.

Tensile Strength	MPa	700
Tensile Modulus	GPa	54
Tensile Strain at Break	%	1.5
Flexural Strength	MPa	470
Flexural Modulus	GPa	51
Flexural Strain at Break	%	1.2
Compressive Strength	MPa	320
Compressive Modulus	MPa	54
Compressive Strain at Break	%	0.7
Density	g/cm^3	1.4

appears. At the same time, a new strain concentration has been created at the interface between the reinforcement and the plate that seems to drive the failure mechanism of the plate.

The assessed numerical models have been used to investigate several combinations of reinforcement strategies. The outcomes of the analysis have highlighted that, for the same quantity of reinforcements, it is more convenient to place them in the surrounding area of the hole.

In conclusion, it is possible to state that with the introduction of carbon fiber reinforcements via additive manufacturing it is possible to change significantly stress and strain fields. It is possible to reduce maximum stress concentration value and change its position within the plate. The large design space offered by the manufacturing process, as well as, the modeling techniques here presented can found application in a systematic optimization of the reinforcement strategies.

Acknowledgment

Dr. Alfonso Pagani acknowledges the support from the European Research Council (ERC) under the European Union's Horizon 2020 research and innovation programme (Grant agreement No. 850437).

Declaration of Competing Interest

The authors declare that they have no known competing financial interests or personal relationships that could have appeared to influence the work reported in this paper.

Appendix A. Material properties

The material properties adopted in the present work are those from the data-sheet provided by the material supplier [33]. Table A.7 reports the mechanical properties of the nylon used as matrix. Table A.8 reports the mechanical properties of the carbon fibers.

References

[1] P. Withey, Fatigue failure of the de havilland Comet i, Eng. Fail. Anal. 4 (2) (1997) 147–154, doi:10.1016/S1350-6307(97)00005-8.
[2] G. Savin, Stress Concentration around Holes, Pergamon Press, 1961.
[3] R. Roark, Formulas for Stress and Strain, McGraw Hill, 1965.
[4] H. Peterson, Stress Concentration Factors, John Wiley & Sons, 1974.
[5] R. Howland, L. Filon, On the stresses in the neighbourhood of a circular hole in a strip under tension, Philos. Trans. R. Soc. Lond. Ser. A: Contain. Pap. Math. Phys. Character 229 (1930), doi:10.1098/rsta.1930.0002.
[6] G. Mekalke, M. Kavade, S. Deshpande, Analysis of a plate with a circular hole by FEM, IOSR J. Mech. Civil Eng. 1 (2013) 25–30.
[7] S. Masrol, W. Siswanto, Stress concentration analysis of plate with circular hole: elasticity theory and finite element comparison, Appl. Mech. Mater. 465 (2014) 1385–1389.
[8] Z. Yang, C.-B. Kim, C. Cho, H.G. Beom, The concentration of stress and strain in finite thickness elastic plate containing a circular hole, Int. J. Solids Struct. 45 (3) (2008) 713–731, doi:10.1016/j.ijsolstr.2007.08.030.
[9] P. Yu, W. Guo, C. She, J. Zhao, The influence of Poisson's ratio on thickness-dependent stress concentration at elliptic holes in elastic plates, Int. J. Fatigue 30 (1) (2008) 165–171, doi:10.1016/j.ijfatigue.2007.02.007.
[10] W. Ko, Stress Concentration Around a Small Circular Hole in the Himat Composite Plate, Tech. Rep. NASA-TM-86038, NASA, 1985.
[11] L. Toubal, M. Karama, B. Lorrain, Stress concentration in a circular hole in composite plate, Compos. Struct. 68 (1) (2005) 31–36, doi:10.1016/j.compstruct.2004.02.016.
[12] A. Khechai, A. Tati, A. Guettala, Finite element analysis of stress concentrations and failure criteria in composite plates with circular holes, Front. Mech. Eng. 9 (3) (2014) 281–294, doi:10.1007/s11465-014-0307-9.
[13] J. Whitney, R. Nuismer, Stress fracture criteria for laminated composites containing stress concentrations, J. Compos. Mater. 8 (3) (1974) 253–265, doi:10.1177/002199837400800303.
[14] S. Meguid, Finite element analysis of defence hole systems for the reduction of stress concentration in a uniaxially-loaded plate with two coaxial holes, Eng. Fract. Mech. 25 (4) (1986) 403–413, doi:10.1016/0013-7944(86)90254-7.
[15] P.E. Erickson, W.F. Riley, Minimizing stress concentrations around circular holes in uniaxially loaded plates, Exp. Mech. 18 (3) (1978) 97–100, doi:10.1007/BF02325003.
[16] U. Jindal, Reduction of stress concentration around a hole in a uniaxially loaded plate, J. Strain Anal. Eng. Des. 18 (2) (1983) 135–141, doi:10.1243/03093247V182135.
[17] Q. Yang, C.F. Gao, Reduction of the stress concentration around an elliptic hole by using a functionally graded layer, Acta Mech. 227 (9) (2016) 2427–2437, doi:10.1007/s00707-016-1620-7.
[18] R. Sburlati, S. Atashipour, S. Atashipour, Reduction of the stress concentration factor in a homogeneous panel with hole by using a functionally graded layer, Compos. Part B: Eng. 61 (2014) 99–109, doi:10.1016/j.compositesb.2014.01.036.
[19] M. Hyer, R. Rust, W. Waters, Innovative Design of Composite Structures: Design, Manufacturing, and Testing of Plates Utilizing Curvilinear Fiber Trajectories, Tech. Rep. NASA-CR-197045, NASA, 1994.
[20] P. Vannucci, Plane anisotropy by the polar method, Meccanica 40 (2005) 437–454, doi:10.1007/s11012-005-2132-z. 4-6 SPEC.
[21] M. Montemurro, An extension of the polar method to the first-order shear deformation theory of laminates, Compos. Struct. 127 (2015) 328–339, doi:10.1016/j.compstruct.2015.03.025.
[22] M. Montemurro, A. Catapano, A general b-spline surfaces theoretical framework for optimisation of variable angle-tow laminates, Compos. Struct. 209 (2019) 561–578, doi:10.1016/j.compstruct.2018.10.094.
[23] P. Crothers, K. Drechsler, D. Feltin, I. Herszberg, T. Kruckenberg, Tailored fibre placement to minimise stress concentrations, Compos. Part A: Appl. Sci. Manuf. 28 (7) (1997) 619–625, doi:10.1016/S1359-835X(97)00022-5.
[24] K. Gliesche, T. Hbner, H. Orawetz, Application of the tailored fibre placement (tfp) process for a local reinforcement on an 'open-hole' tension plate from carbon/epoxy laminates, Compos. Sci. Technol. 63 (1) (2003) 81–88, doi:10.1016/S0266-3538(02)00178-1.
[25] N. van de Werken, H. Tekinalp, P. Khanbolouki, S. Ozcan, A. Williams, M. Tehrani, Additively manufactured carbon fiber-reinforced composites: state of the art and perspective, Addit. Manuf. 31 (2020) 100962, doi:10.1016/j.addma.2019.100962.
[26] B. Brenken, E. Barocio, A. Favaloro, V. Kunc, R.B. Pipes, Fused filament fabrication of fiber-reinforced polymers: a review, Addit. Manuf. 21 (2018) 1–16, doi:10.1016/j.addma.2018.01.002.
[27] A.N. Dickson, J.N. Barry, K.A. McDonnell, D.P. Dowling, Fabrication of continuous carbon, glass and kevlar fibre reinforced polymer composites using additive manufacturing, Addit. Manuf. 16 (2017) 146–152, doi:10.1016/j.addma.2017.06.004.
[28] L. Blok, M. Longana, H. Yu, B. Woods, An investigation into 3d printing of fibre reinforced thermoplastic composites, Addit. Manuf. 22 (2018) 176–186, doi:10.1016/j.addma.2018.04.039.
[29] T.C. Chu, W.F. Ranson, M.A. Sutton, Applications of digital-image-correlation techniques to experimental mechanics, Exp. Mech. 25 (3) (1985) 232–244, doi:10.1007/BF02325092.
[30] Y. Dai, H. Wang, G. Wu, J. Wan, S. Cao, F. Yang, X. He, Behavior investigation of cfrp-steel composite members using digital image correlation, in: M. Sutton, P.L. Reu (Eds.), International Digital Imaging Correlation Society, Springer International Publishing, Cham, 2017, pp. 129–132.
[31] W.D. Pilkey, D.F. Pilkey, Peterson's Stress Concentration Factors, John Wiley & Sons, Inc., 2007, doi:10.1002/9780470211106.
[32] Standard Test Method for Open-Hole Tensile Strength of Polymer Matrix Composite Laminates, ASTM, west conshohocken, PA, 2011. https://cds.cern.ch/record/1484468.
[33] Markforged, Material datasheet (REV 3.2 — 9/9/2019), 2019. http://static.markforged.com/.